An Extreme-Learning-Machine-Based Hyperspectral Detection Method of Insulator Pollution Degree

YAN QIU, GUANGNING WU (ID), (Fellow, IEEE), ZHANG XIAO, YUJUN GUO (ID), (Member, IEEE), XUEQIN ZHANG, (Member, IEEE), AND KAI LIU (ID)
College of Electrical Engineering, Southwest Jiaotong University, Chengdu 611756, China

Corresponding author: Yujun Guo (yjguo@swjtu.edu.cn)

ABSTRACT The on-line detection of insulator pollution degree of transmission lines is important to the prevention and control of flashover. This paper proposed a non-contact detection method of insulator pollution degree based on hyperspectral technique. Firstly, hyperspectral images of the samples with different pollution degrees were obtained by hyper-spectrometer. Secondly, after original hyperspectral images were corrected by black-and-white correction and multiplicative scatter correction, hyperspectral curves from the region of interest (ROI) of corrected images were obtained. Finally, a multiclassification model of extreme learning machine (ELM) was built to realize the pollution degree classification of test samples. The results show that the absorption peak, the position of reflection peak, amplitude and the change trend of the hyperspectral curve obviously change with different kinds of pollution on the surface of silicone rubber, whereas only the amplitude obviously changes with same kind of pollution on the surface of silicone rubber; and the ELM-classification model can accurately and rapidly classify the pollution degree, with the pollution degree classification accuracy of NaCl, $CaSO_4$ and mixed $NaCl$-$CaSO_4$ respectively reaching 95%, 97.5% and 97.5%; and finally The ELM model based on hyperspectral curves data of the artificial pollution samples can classify the surface of insulator umbrellas with different pollution degrees, and the classification accuracy of $CaSO_4$ and mixed $NaCl$-$CaSO_4$ samples respectively are 87.5% and 90%. Consequently, the results of this study prove that hyperspectral technique has considerable potential for the non-contact detection of insulator pollution degree.

INDEX TERMS Hyperspectral technique, insulator, pollution degree, multiplicative scatter correction, extreme learning machine.

I. INTRODUCTION

The flashover of transmission line insulator is the key problem to be solved for the safe and stable operation of electrical power system. Moreover, the loss caused by pollution flashover to the power system is nearly 10 times of the loss caused by lightning flashover [1]. As the transmission line insulators are exposed to the atmospheric environment for a long time, pollution gradually accumulates on the insulators' surface. Under meteorological conditions such as fog, dew, drizzle and acid rain, the electrical strength will obviously decline, which will easily lead to surface discharge of insulators, thus causing pollution flashover. Pollution flashover has two notable characteristics: one is that in the humid weather conditions such as fog, dew, drizzle, many insulators with same creepage distance in the similar environment may flashover simultaneously; the other is that reclosing is hard to succeed, which can result in long-time ground fault. Therefore, pollution flashover can easily cause the system to lose stability leading to large-scale outages. With the rapid development of industry and agriculture, severe weather conditions such as fog-haze and salt-fog happen

The associate editor coordinating the review of this article and approving it for publication was Qiangqiang Yuan.

more frequently, so that pollution problem is more serious. Meanwhile, with the construction of UHV transmission lines, once pollution flashover accident occurs, it will cause greater damage [2]–[5]. Therefore, it is of great significance to effectively determine the pollution degree of insulators and make a targeted insulator cleaning plan according to the judgment results for the prevention and control of pollution flashover.

At present, measurement methods commonly used in insulator pollution degree include equivalent salt deposit density (ESDD), leakage current (LC), surface pollution layer conductivity (SPLC) [6]–[8]. These traditional measurement methods have certain limitations. The ESDD method requires operators to climb up the transmission towers to remove insulators, and then constantly scrub the insulator surface with absorbent cotton immersed in distilled water. The absorbent cotton after each scrub is placed in a quantity of distilled water until the pollution is cleaned, and the whole process is required to avoid the loss of pollution and moisture. So, the whole measurement process is so tedious, which is not suitable for on-line detection. For LC measurement, the power is generally supplied by high-voltage rectifying equipment, and the LC is directly measured by microammeter, which has high requirements on the experimental equipment, environment and the sensitivity of measuring instrument. So, LC measurement will be easily affected by the voltage polarity of power supply, ambient humidity, temperature, etc., and it is difficult to establish a direct relationship with pollution degree. The measurement of SPLC should be carried out under the condition of saturated and damp pollution layer, and need complex measurement equipment, and it is difficult to control the damp condition of the insulators, which is not convenient for field measurement. Spectral analysis technology such as infrared imaging [9], [10], ultraviolet imaging [11], [12] have been widely used in insulator pollution flashover prevention because of the advantage of non-contact detection, but these two methods' spectral resolution is relatively low, and spectrum is narrow (imaging in a particular band). Infrared imaging only reflects the characteristics of insulators' heating, while ultraviolet imaging only reflects the characteristics of insulators' discharge, both of them lacking the complete reflection of insulator pollution state.

Hyperspectral technique is the new technology which combines image and data based on imaging spectroscopy technology, with some advantages such as multiband(up to hundreds of wavebands), high resolution, rich information collected by hyperspectral images and large amounts of data description models, etc. [13], [14]. Hyperspectral technique is mainly used in food detection, agriculture monitoring, resource exploration, archaeological investigation and so on [15]–[19]. S. Shrestha captured hyperspectral images of four tomato varieties and analyzed the data by principal component analysis (PCA) and partial least squares-discriminant analysis (PLS-DA), and the results showed the application prospects of using hyperspectral imaging in varietal identification studies of tomato seeds [16]. Zhang et al. presented

an automatic soil texture classification system using hyperspectral soil signatures and wavelet-based statistical models, and the results showed that the methods are both reliable and robust [18]. Daikos et al. made use of hyperspectral imaging for in-line monitoring of thickness and conversion of white pigmented UV-cured acrylate coatings, proving that hyperspectral imaging has considerable potential for in-line process and quality control [19]. The mature application of hyperspectral technique in other fields and its great potential in on-line detection have attracted our wide attention. In view of the lack of non-contact on-line detection method for insulator pollution, the hyperspectral technique is applied to detect insulator pollution degree for the first time.

This paper aims to study the pollution degree detection method of insulators based on hyperspectral technique. Through obtaining hyperspectral images of artificial samples with different pollution degrees, the full-band hyperspectral curves of the regions of interest in label sample images are extracted after pre-treatment to build an ELM multiclassification model. The full-band data of label samples are taken as training data to classify the pollution degree of artificial samples to be tested. This method is a way of non-contact detection, which can realize undamaged and on-line detection of the pollution degree. The results show that this method has considerable potential for the non-contact detection of insulator pollution degree with high classification accuracy.

II. THE PRINCIPLE OF THE POLLUTION DEGREE DETECTION BASED ON HYPERSPECTRAL TECHNIQUE

A. THE PRINCIPLE OF HYPERSPECTRAL IMAGING TECHNIQUE

With the wide application of hyperspectral technique in various fields, great changes have taken place in the theory, technology and applications. The imaging spectrometer mounted in hyperspectral sensors of different spatial platforms can get hyperspectral data, and simultaneously image the target in ultraviolet, visible, near-infrared and mid-infrared regions of the electromagnetic spectrum in tens to hundreds of continuous spectral bands, as shown in Fig. 1. Hyperspectral
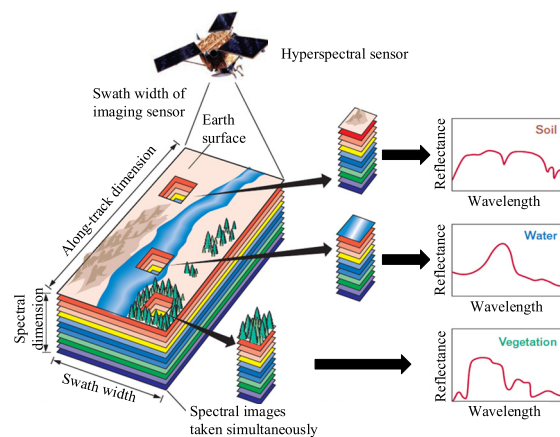

**FIGURE 1.** Schematic of hyperspectral data.

image not only improves the richness of information, but also analyzes and processes the spectral data more reasonably and efficiently [13].

The spectral characteristics of substance are closely related to its inherent physicochemical characteristics, and the absorption and reflection of photons at different wavelengths within the substance are selectively due to the differences in composition and structure. Therefore, the reflectance spectrum of the substance has a "fingerprint" effect, which can distinguish different substance information according to the principle that different substances have different spectra and the same substance has the same spectrum. A complete and continuous spectral curve can better reflect the intrinsic microscopic differences between different substance, which is the physical basis of hyperspectral imaging for fine substance detection.

B. THE PRINCIPLE OF HYPERSPECTRAL DETECTION ON POLLUTION DEGREE

Taking the soluble salt (NaCl) and the slightly soluble salt ($CaSO_4$) which commonly exist in the pollution of insulator surface for example, the pollution of different components shows different reflectance characteristics. According to IEC standard 60815-1 [21], as the non-soluble deposit density (NSDD) in this experiment is set to a fixed value, the four degrees from top to bottom respectively are defined as "light" (denoted by the symbol "I"; ranging from 0.03 mg/cm^2 to 0.06 mg/cm^2) and "medium" (II, 0.06 mg/cm^2-0.10 mg/cm^2), "heavy" (III, 0.10 mg/cm^2-0.25 mg/cm^2), "very heavy" (IV, >0.25 mg/cm^2). As shown in Fig. 2(a), the sample NaCl forms continuous curves at 400-1000 nm. Due to the pollution amount of different pollution degrees, the reflectance at 400-980 nm shows a rule that the reflectance decreases with the increase of pollution degree. This is because of the particularity of NaCl that crystals are formed during the natural drying process. With the increasing ESDD, the content of NaCl on the surface of the insulation sheet increases, and the formed crystals increase as well, so that the surface pollution increases the absorption of light and reduces the reflection, resulting in the decline of overall reflectance.

The sample $CaSO_4$ forms continuous curves at 400–1000 nm, and the four degrees from bottom to top respectively are I, II, III, IV. This is because $CaSO_4$ does not form crystals during the natural drying process. As the content of $CaSO_4$ increases, the surface pollution reduces the absorption of light and increases the reflection. The reflectance at 400-980 nm shows a rule that the reflectance increases with the increase of pollution degree. As shown in Fig. 2(b), there are significant differences in the positions of absorption and reflection peak when the pollution not completely covering and completely covering the base material. When the pollution completely covering the base material (curves corresponding to III, IV), the offset of absorption and reflection peak is smaller.
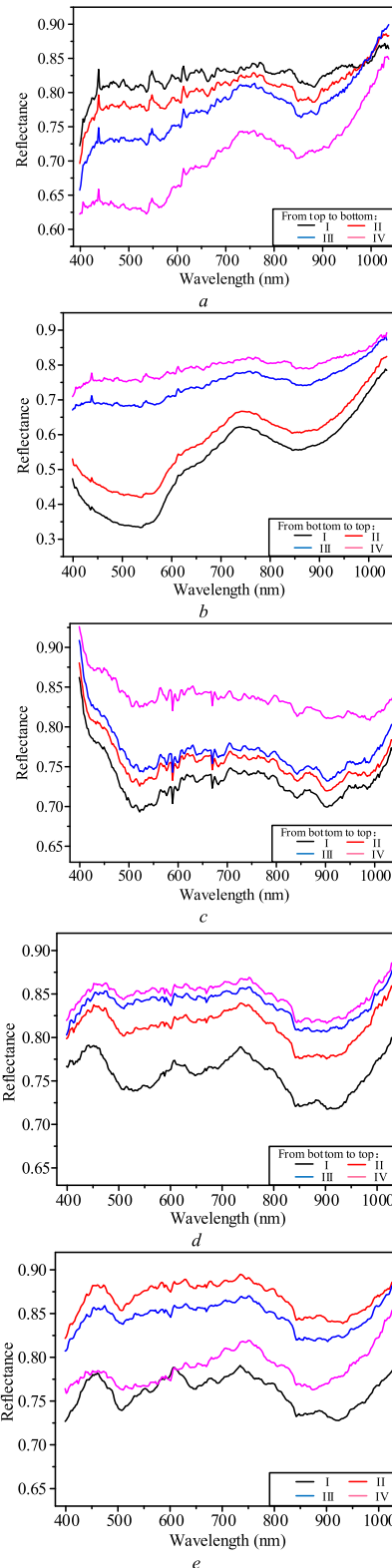
FIGURE 2. Hyperspectral curves of different pollution with different degrees. (a) sample NaCl. (b) sample $CaSO_4$. (c) sample mixed NaCl-$CaSO_4$ (the ratio of NaCl to $CaSO_4$ is 1 to 2). (d) sample mixed NaCl-$CaSO_4$ (1:1). (e) sample mixed NaCl-$CaSO_4$ (2:1).

When NaCl and $CaSO_4$ were mixed and the ratio of NaCl was 1/3 and 1/2 of samples in different content proportion, the reflectance of these samples at 400-980 nm

increases with the increase of pollution degree, showing the same change trend as that of sample CaSO$_4$. As shown in Fig. 2(c) and Fig. 2(d), The four degrees from bottom to top respectively are I, II, III, IV. This is because when the content of NaCl is relatively low, fewer crystals are formed, and its influence on the spectral curves is insufficient to make the reflectance rule similar to that of sample NaCl. As shown in Fig. 2(e), when the ratio of NaCl was 2/3, the reflectance of these samples at 400-980 nm increases with the decrease of pollution degree, gradually showing the same change trend as that of sample NaCl. The above reflectance characteristics can be used as the theoretical basis for the division of pollution degrees.

III. EXPERIMENT METHOD
A. HYPERSPECTRAL TEST PLATFORM
The hyperspectral test platform is composed of the hyperspectral imaging system (hyper-spectrometer, computer, etc.), the symmetrical double light sources, and a standard white board with reflectance nearly about 100%. The system can be used to obtain hyperspectral images of experimental samples. In the experiment, the hyper-spectrometer (parameters shown in Table I) was mounted on a tripod with a distance of 120 cm from lens to the sample and a downward angle of 45°. As shown in Fig. 3, the light sources were symmetrically placed on both sides of the samples. The samples were placed in the imaging area for hyperspectral acquisition, and the data were transmitted to the computer via the USB line of the hyper-spectrometer. The experiment was carried out

TABLE 1. Parameters of hyper-spectrometer.

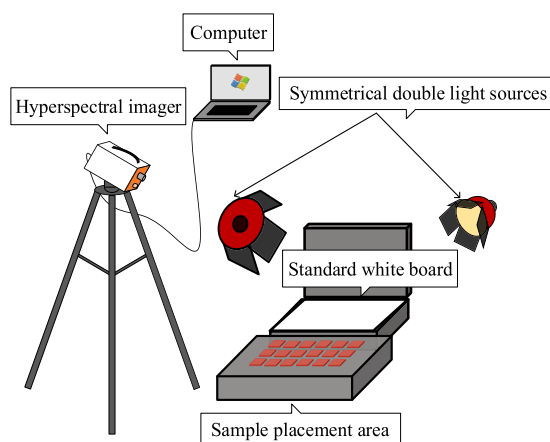| Main parameters	Values
Model	GaiaField-F-V10
Wavelength range	400-1000 nm
Spectral resolution	2.8 nm
CCD pixel	1392×1040

FIGURE 3. Schematic of hyperspectral testing platform.

under the conditions of temperature 18–25° and humidity 30%–80%.

B. SAMPLE PREPARATION
The experimental samples were divided into three groups, and samples were prepared according to the IEC standard 61245 [20] and IEC standard 60815-1 [21], and the silicone rubber insulation sheet (5 cm × 5 cm) was used as base material. Since the pollution of insulator often contains NaCl, CaSO$_4$ and other components, NaCl is generally 10% to 30% and CaSO$_4$ accounts for 20% to 60%. Although CaSO$_4$ is a slightly soluble substance, it has a significant effect on the flashover voltage [22], [23]. Therefore, the first group selects NaCl as the leaching solute; the second group selects CaSO$_4$ as the leaching solute; the third group selects mixed NaCl and CaSO$_4$ as the leaching solute to prepare the mixed artificial effluent of different solute and kaolin.

According to the solid layer method recommended in the standard [20], samples of four pollution degrees were prepared for each group. As shown in Fig. 4(a), the first group of sample R was labelled as tag sample R1, R2, R3, R4, and test sample R5, R6, R7, R8. Solutions of different volume conductivity are prepared to uniformly make the mixture adhere to the silicone rubber insulation sheet. The ESDD corresponding to the samples with different pollution degrees respectively were 0.04 mg/cm^2, 0.08 mg/cm^2, 0.15 mg/cm^2 and 0.30 mg/cm^2, and the NSDD was 0.10 mg/cm^2. As shown in Fig. 4(b), the second group of sample T was labelled as tag sample T1, T2, T3, T4, and test sample T5, T6, T7, T8. The ESDD corresponding to the samples with different pollution degrees were 0.05 mg/cm^2, 0.10 mg/cm^2, 0.18 mg/cm^2 and 0.30 mg/cm^2, and the NSDD was 0.10 mg/cm^2. As shown in Fig. 4(c), the third group of sample O, P and Q were labelled as tag sample O (P or Q) 1-4, and test sample O (P or Q) 5-8. Where, the ratio of NaCl to CaSO$_4$ for O is 1:2; that for P is 1:1, and that for Q is 2:1. The ESDD corresponding to the samples with different pollution degrees were 0.06 mg/cm^2, 0.10 mg/cm^2, 0.20 mg/cm^2, 0.35 mg/cm^2, and the NSDD was 0.10 mg/cm^2. Three groups of samples were naturally dried for 24 hours.

IV. RESULTS AND ANALYSIS
A. SAMPLE SPECTRUM ACQUISITION
Images of each group of samples were collected separately in the laboratory via the GaiaField-F-V10 hyper-spectrometer. The pixel reflectance of samples with different pollution degrees was extracted from the hyperspectral image of artificial pollution samples, and the wavelength was taken as the abscissa and the reflectance was taken as the ordinate. Among them, 10 sets of data were extracted from each tag sample of three groups of samples as training data, and same process for test data from test samples. Therefore, in the spectrum acquisition of NaCl or CaSO$_4$, there were 40 sets of training data and 40 sets of test data, each accounting for 50%. In the spectrum acquisition of mixed NaCl-CaSO$_4$, there were a
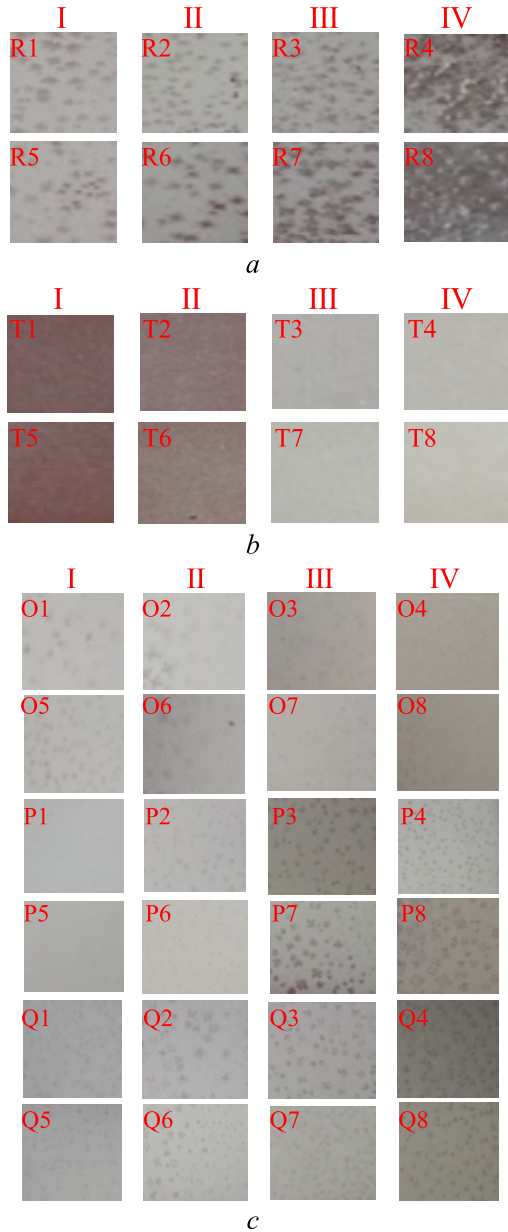
FIGURE 4. Artificial pollution samples made by solid layer method.(a) sample NaCl. (b) sample CaSO$_4$. (c) sample mixed NaCl-CaSO$_4$.

total of 120 sets of training data and 120 sets of test data, each accounting for 50%. This is because three different proportions of sample mixed NaCl-CaSO$_4$ were prepared.

The hyperspectral image reflectance obtained by the hyperspectrometer forms a continuous spectral curve in the wavelength range of 400–1000 nm, and the samples with different pollution degrees correspond one-to-one with the spectral curves. The curves can be further analysed by algorithms.

B. HYPERSPECTRAL PRETREATMENT

Since the light distribution may be uneven and image noise and dark current may exist in the band with weak light distribution in the process of collecting hyperspectral images,

it is often necessary to preprocess the original image for subsequent analysis of hyperspectral data.

1) BLACK-AND-WHITE CORRECTION

In order to overcome the influence of image noise and dark current in the band with weak light distribution, when collecting the sample hyperspectral image, the standard white board was scanned at the same time to collect the white calibration image with reflectance nearly about 100%, and then the black calibration image with the reflectance of 0 was collected under the lens cover. The hyperspectral data correction can be realized by using black-and-white correction. Correction algorithm is as follows:

$$R_{ci} = \frac{Sample_{ci} - dark_{ci}}{White_{ci} - dark_{ci}} \quad (1)$$

where $Sample_{ci}$ is original spectral image data; $Dark_{ci}$ is black calibrated image data; $White_{ci}$ is white calibration image data; R_{ci} is black-and-white corrected image data. As shown in Fig. 5, the burr of spectral curves relatively decreased, and the curves were smoother after black-and-white correction.
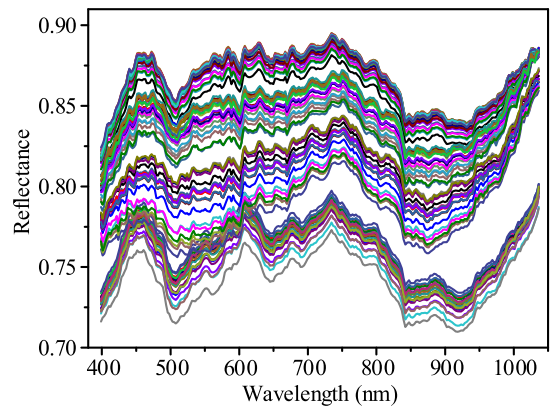
FIGURE 5. Hyperspectral curves after black-and-white correction.

2) MULTIPLICATIVE SCATTER CORRECTION

Multiple scattering correction is a commonly used data processing method of multiple wavelength calibration modelling at the present, after the correction of spectral data can effectively eliminate the scattering effects, and enhance the relationship between spectral data and the spectral absorption information of component and content [24]. In this paper, multiplicative scatter correction is used to correct the original hyperspectral image data.

Firstly, the average spectrum of samples was calculated, which was used as the standard spectrum. The hyperspectral images of each group of samples and the standard spectrum were performed with unary linear regression, and the linear translation (regression constant) and the gradient (regression coefficient) of each spectrum related to the standard spectrum were obtained. Subtract the linear translation from the original spectrum data of each sample and then the data is

divided by the regression coefficient to correct the relative inclination of the baseline, so that the translation and offset of baseline of each spectrum were corrected with the reference of standard spectrum. The spectral absorption information corresponding to component and content of samples did not have any influence on the whole process of data processing, so the signal-to-noise ratio of spectrum was improved. The following is the specific algorithm process:

Calculation of average spectrum:

$$\overline{\mathbf{A}}_{i,j} = \frac{\sum_{i=1}^{n} \mathbf{A}_{i,j}}{n} \qquad (2)$$

Unary linear regression:

$$\mathbf{A}_i = m_i \overline{\mathbf{A}} + b_i \qquad (3)$$

Multiplicative scatter correction:

$$\mathbf{A}_{i(MSC)} = \frac{(\mathbf{A}_i - b_i)}{m_i} \qquad (4)$$

where *A* is a spectral data matrix of $n \times p$; n is the number of selected samples; p is the number of wavelengths of spectrum; i is the ith sample; j is the jth band; $\overline{A}$ is the average spectral vector obtained by averaging the original spectrum at each band of all samples; A_i is a matrix of $1 \times p$, representing a single spectrum vector; m_i and b_i respectively are relative migration coefficient and translation amount obtained by the unary linear regression between A_i and $\overline{A}_{i(MSC)}$ is the hyperspectral curve after MSC correction.

As shown in Fig. 6, the dispersion of samples' spectral curves decreased and appeared to converge after multiplicative scatter correction. It was proved to be convenient for subsequent classification of pollution degrees.
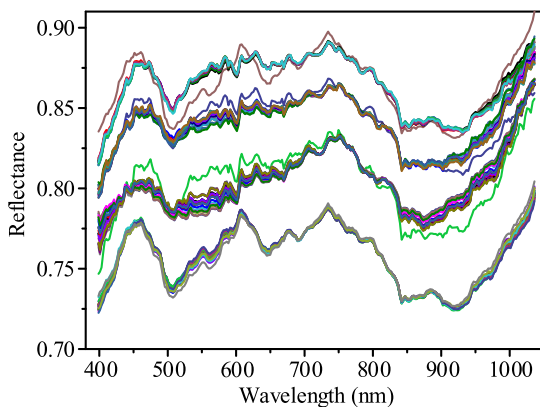

FIGURE 6. Hyperspectral curves after multiplicative scatter correction.

C. CLASSIFICATION OF POLLUTION DEGREES BASED ON THE ELM MODEL

ELM is a kind of machine learning algorithm based on feed-forward neuron network. Its main characteristic is that parameters of hidden layer nodes can be randomly or artificially given without adjustment, and the learning process

only needs to calculate the output weight. Therefore, ELM has the advantages of high learning efficiency and strong generalization ability [25], [26]. Samat *et al.* introduced ELM for hyperspectral image classification and the results showed that the proposed ensemble algorithms produced excellent classification performance in different scenarios with respect to spectral and spectral-spatial feature sets [27]. Zhou *et al.* proposed two spatial-spectral composite kernel (CK) ELM classification methods, which worked fine for hyperspectral image classification [28]. Due to the high efficiency and accuracy of the classification of extreme learning machine, the ELM theory [29], [30] was adopted into the problem of insulator pollution degree classification. Considering that this is a multi-classification problem, an ELM multi-classification model was designed. Since the classification speed of extreme learning machine is very fast, only the output weight β needs to be calculated. The time complexity is $O(min(L^3, N^3))$, where L is the number of hidden neurons (set as 20 in this paper) and N is the number of training samples. We use the method of randomly generating hidden layer nodes and then obtain the solution of β in formula (5) according to the label samples data to complete the establishment of the entire neural network.
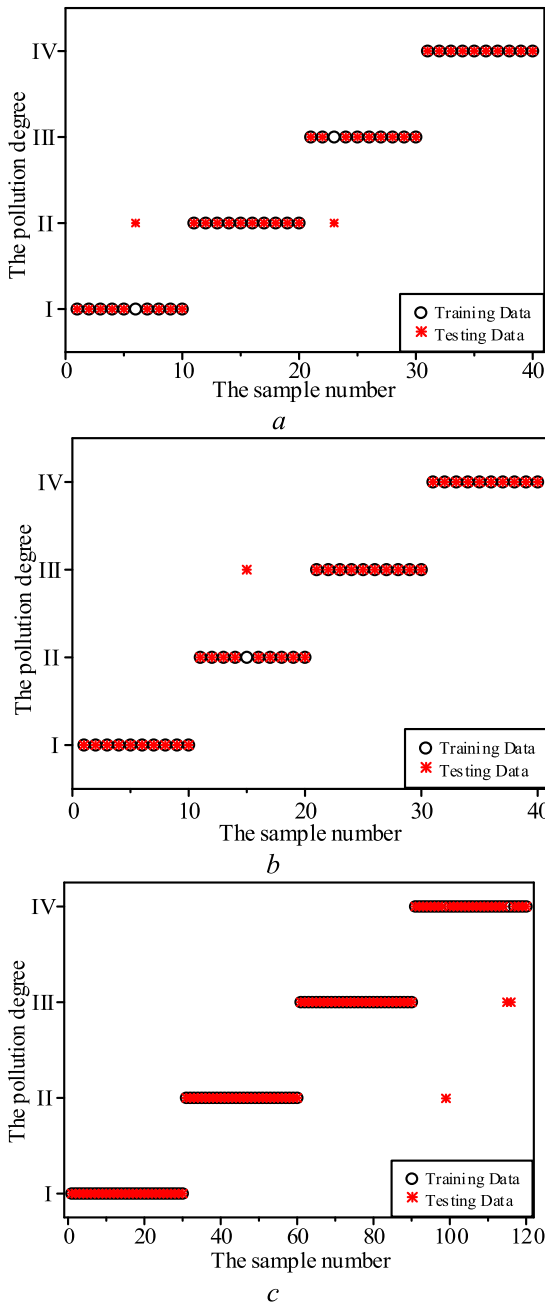
$$\mathbf{T} = \mathbf{H} \bullet \boldsymbol{\beta} \qquad (5)$$

where *T* is the pollution degree labels; *H* is the output matrix of hidden layer of the neural network; and β is the weight of each node of hidden layer with the output node.

In this paper, the classification objectives were four pollution degrees. As the spectral curves had obvious characteristics in the entire band reflectance, the reflectance values of 256 bands were taken as the input, and the output was the classification result of test sample data, as shown in Fig. 7.

In Fig. 7, the ordinate represents the pollution degree I, II, III and IV, and the abscissa represents the number of test sample data. In Fig. 7(a) and (b), the true pollution degree of sample 1–10 are I; sample 11–20 are II; sample 21–30 are III, and sample 31–40 are IV. In Fig. 7(c), the true pollution degree of sample 1-30 are I; sample 31-60 are II; sample 61–90 are III, and sample 91–120 are IV. Fig. 7(a) shows that there are errors in the classification of sample 6 and 23, so that the accuracy is 95%. Fig. 7(b) shows that there is an error in the classification of sample 15, so that the accuracy is 97.5%. And Fig. 7(c) shows that there are errors in the classification of sample 99, 115 and 116, so that the accuracy is 97.5%. Therefore, it is proved that the ELM classification model can accurately classify substances with different pollution degrees.

D. MODEL VERIFICATION

In this paper, insulator FQJG2-30/16-400-M was used as an example to verify the model. Through artificial pollution test [20], pollution was deposited on composite insulator umbrella, as shown in Fig. 8. In Fig. 8(a), pollution on insulator was $CaSO_4$ and kaolin; In Fig. 8(b), pollution on insulator was NaCl, $CaSO_4$ and kaolin. Because the size

FIGURE 7. The degree classification results of different pollution. (a) sample NaCl. (b) sample CaSO₄. (c) sample mixed NaCl-CaSO₄.

each solution are measured, and then the ESDD of each area is obtained through formula conversion. After that, the above pollution solution was filtered, dried and weighed, and the NSDD was calculated. The measurement results were as follows. In Fig. 8(a), the ESDD of insulator umbrella 1 was 0.05 mg/cm^2, and the NSDD was 0.10 mg/cm^2, corresponding to pollution degree I. The ESDD of umbrella 2 was 0.09 mg/cm^2 and the NSDD was 0.08 mg/cm^2, corresponding to pollution degree II. The ESDD of insulator umbrella 3 was 0.18 mg/cm^2, and the NSDD was 0.15 mg/cm^2, corresponding to pollution degree III. The ESDD of umbrella 4 was 0.33 mg/cm^2 and the NSDD was 0.17 mg/cm^2, corresponding to pollution degree IV. In Fig. 8(b), the ESDD of insulator umbrella 1 was 0.05 mg/cm^2, and the NSDD was 0.09 mg/cm^2, corresponding to pollution degree I. The ESDD of umbrella 2 was 0.07 mg/cm^2 and the NSDD was 0.15 mg/cm^2, corresponding to pollution degree II. The ESDD of insulator umbrella 3 was 0.21 mg/cm^2, and the NSDD was 0.13 mg/cm^2, corresponding to pollution degree III. The ESDD of umbrella 4 was 0.35 mg/cm^2 and the NSDD was 0.18 mg/cm^2, corresponding to pollution degree IV.
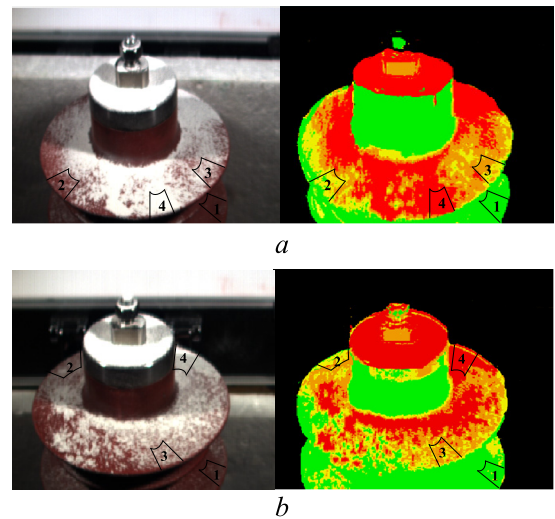
FIGURE 8. Pollution distribution of artificially polluted composite insulator. (a) insulator polluted by CaSO₄. (b) insulator polluted by mixed NaCl-CaSO₄.

After pollution accumulated on the insulator, its hyperspectral image was collected, and then black-and-white correction and multiplicative scatter correction were applied to get hyperspectral curves of umbrella 1–4. each group had 10 spectral curves data as the test data of the ELM classification model established in section 4.2, classification results as shown in Fig. 9. Among them, sample 1–10 were taken from umbrella 1 with true pollution degree I. Sample 11–20 were taken from umbrella 2 with true pollution degree II. Sample 21–30 were taken from umbrella 3 with true pollution degree III. Sample 31–40 were taken from umbrella 4 with true pollution degree IV. The classification results in Fig. 9(a) indicated that the classification of sample 11, 12, 17, 24
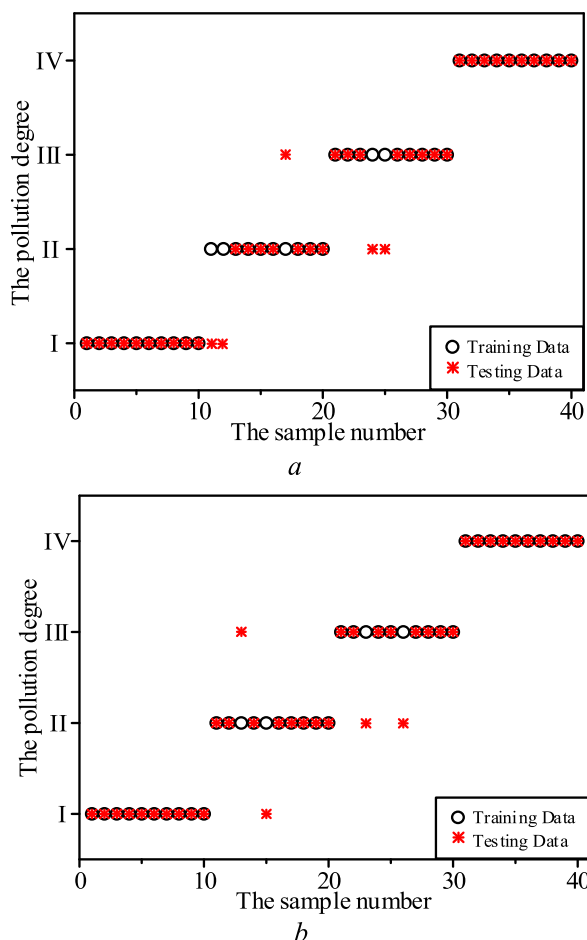
of insulator's umbrella was different from that of silicone rubber insulation sheet, only cleaned the fan-shaped area of insulator's umbrella which had same size with silicone rubber insulation sheet (5 cm×5 cm) with distilled water. According to the measurement method of ESDD and NSDD introduced in the annex C of IEC standard 60815-1 [21], the ESDD and NSDD of the polluted insulator is measured. The absorbent cotton immersed in distilled water is used to continuously scrub the insulator surface, and the pollution of each area is dissolved in the same amount of distilled water respectively. After fully dissolved, the conductivity and temperature of

FIGURE 9. The degree classification results of artificially polluted composite insulator. (a) insulator polluted by $CaSO_4$. (b) insulator polluted by mixed $NaCl-CaSO_4$.

and 25 is wrong, with an accuracy rate of 87.5%. Fig. 9(b) indicated that the classification of sample 13, 15, 23 and 26 is wrong, with an accuracy rate of 90%. Compared with section 4.2, the accuracy is decreased, as shown in Fig. 8. This is because the pollution distribution of artificially polluted insulator was uneven. Hyperspectral data was taken from local area, reflecting the pollution degree of local area, but the pollution degree measured of the fan-shaped area was the average for the area. Therefore, the pollution degree measured might be a little different with that expressed by hyperspectral data, resulting deviations in part of the predicted results.

V. CONCLUSION

This paper studied the detection method of insulator pollution degrees based on hyperspectral technique. The following conclusions can be drawn.

Firstly, the absorption peak, the position of reflection peak, amplitude and the change trend of the hyperspectral curve have differences with different kinds, proportions and degrees of pollution. Secondly, The ELM-classification model based on the artificial pollution samples can accurately and rapidly classify the pollution degrees of a mixture of different salts and the surface of insulator umbrellas (the pollution distribution is uneven), which provides a technical reference for on-line measurement of insulator pollution degrees. Furthermore, in order to make hyperspectral technique better applied to the on-the-spot detection of insulator pollution, the identification of principal components and the classification of pollution degrees of natural pollution based on the hyperspectral features should be further studied.

REFERENCES

[1] D. Wang, A. Xu, P. Liu, and T. Cui, "Flashover mechanism and prevention measures of polluted insulators in power system," in *Proc. Asia–Pacific Power Energy Eng. Conf.*, Wuhan, China, Mar. 2011, pp. 1–4.

[2] Z. Zhang, X. Jiang, C. Sun, J. Hu, and H. Huang, "Study of the influence of test methods on DC pollution flashover voltage of insulator strings and its flashover process," *IEEE Trans. Dielectr. Electr. Insul.*, vol. 17, no. 6, pp. 1787–1795, Dec. 2010.

[3] L. Yang, F. Zhang, Z. Wang, X. Jiang, Y. Hao, L. Li, Y. Liao, and F. Zhang, "Evaluation of wetting condition and its effects on pollution flashover voltage of aerodynamic insulators," *IEEE Trans. Dielectr. Electr. Insul.*, vol. 23, no. 5, pp. 2875–2882, Oct. 2016.

[4] Y. Guo, X. Jiang, Y. Liu, Z. Meng, and Z. Li, "AC flashover characteristics of insulators under haze–fog environment," *IET Gener., Transmiss. Distrib.*, vol. 10, no. 14, pp. 3563–3569, Oct. 2016.

[5] Z. Zhang, D. Zhang, W. Zhang, C. Yang, X. Jiang, and J. Hu, "DC flashover performance of insulator string with fan-shaped non-uniform pollution," *IEEE Trans. Dielectr. Electr. Insul.*, vol. 22, no. 1, pp. 177–184, Feb. 2015.

[6] W. Cai, H. Deng, G. Zhou, J. Wang, and F. Yang, "Online measurement of equivalent salt deposit density by using optical technology," *IEEE Trans. Dielectr. Electr. Insul.*, vol. 20, no. 2, pp. 409–413, Apr. 2013.

[7] I. Ramirez, R. Hernandez, and G. Montoya, "Measurement of leakage current for monitoring the performance of outdoor insulators in polluted environments," *IEEE Elect. Insul. Mag.*, vol. 28, no. 4, pp. 29–34, Jul. 2012.

[8] L. Van Wyk, J. P. Holtzhausen, and W. L. Vosloo, "Surface conductivity as an indication of the surface condition of non-ceramic insulators," in *Proc. IEEE AFRICON*, Stellenbosch, South Africa, Sep. 1996, pp. 485–488.

[9] L. Jin, Z. Tian, J. Ai, Y. Zhang, and K. Gao, "Condition evaluation of the contaminated insulators by visible light images assisted with infrared information," *IEEE Trans. Instrum. Meas.*, vol. 67, no. 6, pp. 1349–1358, Jun. 2018.

[10] X. Jiang and Q. Xia, "Influence of contamination on deteriorated insulators detection with infrared imaging method," in *Proc. Int. Conf. High Voltage Eng. Appl.*, New Orleans, LA, USA, Oct. 2010, pp. 457–460.

[11] F. Lu, S. Wang, and H. Li, "Insulator pollution grade evaluation based on ultraviolet imaging and fuzzy logic inference," in *Proc. Asia–Pacific Power Energy Eng. Conf.*, Chengdu, China, Mar. 2010, pp. 1–4.

[12] Z. Zhang, W. Zhang, D. Zhang, Y. Xiao, J. Deng, and G. Xia, "Comparison of different characteristic parameters acquired by UV imager in detecting corona discharge," *IEEE Trans. Dielectr. Electr. Insul.*, vol. 23, no. 3, pp. 1597–1604, Jun. 2016.

[13] Y. Chen, H. Jiang, C. Li, X. Jia, and P. Ghamisi, "Deep feature extraction and classification of hyperspectral images based on convolutional neural networks," *IEEE Trans. Geosci. Remote Sens.*, vol. 54, no. 10, pp. 6232–6251, Oct. 2016.

[14] H. Erives and G. J. Fitzgerald, "Automatic subpixel registration for a tunable hyperspectral imaging system," *IEEE Geosci. Remote Sens. Lett.*, vol. 3, no. 3, pp. 397–400, Jul. 2006.

[15] M. Huang and R. Lu, "Apple mealiness detection using hyperspectral scattering technique," *Postharvest Biol. Technol.*, vol. 58, no. 3, pp. 168–175, Aug. 2010.

[16] S. Shrestha, M. Knapič, U. Žibrat, L. C. Deleuran, and R. Gislum, "Single seed near-infrared hyperspectral imaging in determining tomato (Solanum lycopersicum L.) seed quality in association with multivariate data analysis," *Sens. Actuators B, Chem.*, vol. 237, pp. 1027–1034, Dec. 2016.

[17] B. Bahrambeygi and H. Moeinzadeh, "Comparison of support vector machine and neutral network classification method in hyperspectral mapping of ophiolite mélanges—A case study of east of Iran," *Egyptian J. Remote Sens. Space Sci.*, vol. 20, no. 1, pp. 1–10, Jun. 2017.

[18] X. Zhang, N. H. Younan, and C. G. O'Hara, "Wavelet domain statistical hyperspectral soil texture classification," *IEEE Trans. Geosci. Remote Sens.*, vol. 43, no. 3, pp. 615–618, Mar. 2005.

[19] O. Daikos, K. Heymann, and T. Scherzer, "Monitoring of thickness and conversion of thick pigmented UV-cured coatings by NIR hyperspectral imaging," *Prog. Organic Coat.*, vol. 125, pp. 8–14, Dec. 2018.

[20] *Artificial Pollution Tests on High-Voltage Ceramic and Glass Insulators to Be Used on D.C. Systems*, IEC Standard 61245, 2015.

[21] *Selection and Dimensioning of High-Voltage Insulators Intended for Use in Polluted Conditions—Part 1: Definitions, Information and General Principles*, IEC Standard 60815-1, 2008.

[22] Z.-J. Zhang, X.-L. Jiang, and C.-X. Sun, "Present situation and prospect of research on flashover characteristics of polluted insulators," *Power Syst. Technol.*, vol. 30, no. 2, pp. 35–40, Jan. 2006.

[23] L. J. Williams, J. H. Kim, Y. B. Kim, N. Arai, O. Shimoda, and K. C. Holte, "Contaminated insulators-chemical dependence of flashover voltages and salt migration," *IEEE Trans. Power App. Syst.*, vol. PAS-93, no. 5, pp. 1572–1580, Sep. 1974.

[24] Y. J. Lu, Y. L. Qu, and M. Song, "Research on the correlation chart of near infrared spectra by using multiple scatter correction technique," *Spectrosc. Spec. Anal.*, vol. 27, no. 5, pp. 877–880, May 2007.

[25] Y. Sönmez, T. Tuncer, H. Gökal, and E. Avcı, "Phishing Web sites features classification based on extreme learning machine," in *Proc. 6th Int. Symp. Digit. Forensic Secur. (ISDFS)*, Antalya, Turkey, Mar. 2018, pp. 1–5.

[26] M. Bucurica, R. Dogaru, and I. Dogaru, "A comparison of extreme learning machine and support vector machine classifiers," in *Proc. IEEE Int. Conf. Intell. Comput. Commun. Process. (ICCP)*, Cluj-Napoca, Rumania, Sep. 2015, pp. 471–474.

[27] A. Samat, P. Du, J. Y. Li, L. Cheng, and S. Liu, "E2LMs: Ensemble extreme learning machines for hyperspectral image classification," *IEEE J. Sel. Topics Appl. Earth Observ. Remote Sens.*, vol. 7, no. 4, pp. 1060–1069, Apr. 2014.

[28] Y. Zhou, J. Peng, and C. L. P. Chen, "Extreme learning machine with composite kernels for hyperspectral image classification," *IEEE J. Sel. Topics Appl. Earth Observat. Remote Sens.*, vol. 8, no. 6, pp. 2351–2360, Jun. 2015.

[29] G.-B. Huang, H. Zhou, X. Ding, and R. Zhang, "Extreme learning machine for regression and multiclass classification," *IEEE Trans. Syst., Man, Cybern. B, Cybern.*, vol. 42, no. 2, pp. 513–529, Apr. 2012.

[30] N.-Y. Liang, G.-B. Huang, P. Saratchandran, and N. Sundararajan, "A fast and accurate online sequential learning algorithm for feedforward networks," *IEEE Trans. Neural Netw.*, vol. 17, no. 6, pp. 1411–1423, Nov. 2006.

ZHANG XIAO was born in Sichuan, China, in 1995. He received the B.Eng. degree from Northeast Electric Power University, Jilin, in 2017. He is currently pursuing the M.E. degree with Southwest Jiaotong University. His research interests include high voltage and external insulation.
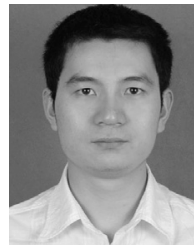
YUJUN GUO (M'18) was born in Hubei, China, in 1989. He received the B.Sc. degree in electrical engineering from the Huazhong University of Science and Technology, Wuhan, in 2011, and the Ph.D. degree in electrical engineering from Chongqing University, Chongqing, in 2017. He is currently a Lecturer with the School of Electrical Engineering, Southwest Jiaotong University. His research interests include outdoor insulation and the protection of transmission lines.

XUEQIN ZHANG (M'10) received the B.Sc. and Ph.D. degrees in electrical engineering from Southwest Jiaotong University, Chengdu, China, in 2002 and 2008, respectively. She was with the Research and Development Center, Toshiba Corporation, Japan, for five years. She is currently an Associate Professor with the School of Electrical Engineering, Southwest Jiaotong University. Her research interests include high voltage and insulation technology. She is a member of CIGRE.

YAN QIU was born in Sichuan, China, in 1995. She received the B.Eng. degree from Southwest Jiaotong University, Chengdu, in 2017, where she is currently pursuing the M.E. degree. Her research interests include high voltage and the external insulation of transmission lines.

GUANGNING WU (M'97–SM'07–F'18) was born in Nanjing, China, in 1969. He received the B.Sc., M.Sc., and Ph.D. degrees in electrical engineering from Xi'an Jiaotong University, in 1991, 1994, and 1997, respectively. He is currently a Professor with the School of Electrical Engineering, Southwest Jiaotong University. His research interests include condition monitoring, fault diagnosis, and insulation life-span evaluation for electrical equipment.

KAI LIU was born in Guizhou, China, in 1990. He received the B.Sc. degree in electrical engineering from the University of Electronic Science and Technology of China, Chengdu, in 2013, and the Ph.D. degree in electrical engineering from Chongqing University, Chongqing, in 2018. He is currently a Lecturer with the School of Electrical Engineering, Southwest Jiaotong University. His research interests include multiple physical field calculations and state diagnosis for electrical equipment.

● ● ●